Relationship between Solid-State Molecular Motion and Morphology for Ultrahigh Molecular Weight Polyethylene Crystallized under Different Conditions

Hiroki Uehara,* Takeshi Yamanobe, and Tadashi Komoto

Department of Chemistry, Gunma University, Kiryu, Gunma 376-8515, Japan

Received November 9, 1999; Revised Manuscript Received March 3, 2000

ABSTRACT: Morphological effects on molecular mobility have been studied for solid ultrahigh molecular weight polyethylenes (UHMW-PE) crystallized from the melt and from solution or during polymerization. On the basis of transmission electron microscopic (TEM) observation, a crystalline domain structure was well identified for nascent UHMW-PE powders, which is quite different from regular lamellar stacking for solution-crystallized samples and the usual spherulites for melt-crystallized samples. Nuclear magnetic resonance (NMR) results showed that the amorphous chains between these crystalline domains in nascent powders were constrained, as well as those sandwiched between stacked crystalline lamellae for the solution-crystallized sample. Also, the existence of three regimes was recognized in the relaxation behavior of the crystalline phase, as revealed by ^{1}H pulse NMR measurements. In process 1 (heating from room temperature), activation of molecular motion at the boundary between crystal/amorphous regions takes place. During process 2 (above the critical temperature of 60−90 °C), the crystallinity increases with the acceleration of the entire molecular motion caused by sliding of molecular chains in the crystalline region. Further raising the temperature (process 3) leads to the start of sample melting. These relaxation mechanisms suggest that the accelerated molecular motion in the crystal/amorphous boundaries initiates following lamellar thickening without passing the melt state.

Introduction

The structure/property relationship of semicrystalline polymers has been discussed for decades but not fully interpreted. Problems lie in an analytical difficulty caused by the complicated combination of crystalline and amorphous phases, including their contents, arrangements, difference in physical properties (electron density, mechanical, and thermal properties and so on) and the usual existence of an interface region between them. For example, each method for crystallinity determination, such as thermal analysis, density, and X-ray measurements, focuses on its own view scale, namely, "where is the borderline between crystalline and amorphous" in terms of physical properties. This is one of the reasons why the crystallinity evaluations by different methods often disagree with each other. Further, mechanical or viscoelastic measurements also suffer difficulty in resolution of each contribution among these combined phases, which always requires several assumptions, "how much depends on each phase". An advantage of NMR measurements is attributed to the ability of NMR for simultaneous estimation of both phase contents and properties (relaxation times) on the same scale, which is quite different from the usual combination of the results obtained by a few analytical methods.

These crystalline and amorphous phases are independently detectable as separated peaks by ^{13}C NMR spectra. However, the relative ^{13}C peak intensities of these phases significantly depend on experimental conditions such as recycling time, contact time, and so on. Further, ^{13}C NMR measurements are time-consuming because of their low sensitivities. In addition, to discuss the phase separation, the effect of spin diffusion cannot be negligible. Taking these factors into consideration, analysis of the proton NMR free induction decay (FID) is suitable for better understanding of the structure/property relationship in this work.

The difficulties of ^{1}H NMR analysis are concerned with the relaxation curve shape of FID.[1] For spin−spin relaxation, the FID exhibits a single-exponential curve in the PE melt with low MW.[2−5] The relaxation curve shape of amorphous molecular motion still retains the combined exponential types on cooling. However, as crystallinity increased, the curve contains crystalline relaxation having beats on FID,[6−12] which cannot be represented by any exponential functions. This phenomenon is well-known for inorganic materials.[13−15] These crystalline FIDs were characterized by multiplication of Gaussian and sine functions.[13] The other type of analytical function for the crystalline phase is that Fourier transformed from a Pake-doublet broad-line spectrum.[16−18] Such doublet spectra on a frequency scale have been observable on ^{1}H NMR for smaller molecules in the solid at low temperature, where proton pairs are isolated from each other.[18] Recently, Kristiansen et al.[10−12] applied a theoretical Fourier transformation of this doublet function to phase analysis for PE and polypropylene.

The curve fitting for observed FIDs also gives the individual spin−spin relaxation characteristics in different phases: crystalline, amorphous, and interfacial.[6,8−12] Such a resolution into several components has been long attempted on a broad-line spectrum of solid PE.[19−22] These results will reflect the sample morphologies. For semicrystalline polymers, quite different morphologies can be obtained, depending on the crystallization conditions.[23,24] Considering the preparation procedures, a solution-crystallized sample is composed of single crystals. A melt-crystallized sample has the usual spherulite structure, where lamellae grow from the center with

* To whom correspondence should be addressed.

10.1021/ma9918957 CCC: $19.00
Published on Web 06/02/2000

some distortion. However, detailed information on the structural origin of the nascent powder as-polymerized is absent. Combination of results for solution- and melt-crystallized samples will realize the relationship between ^{1}H NMR relaxation characteristics and sample morphologies. It is expected that this concept can be extended to the structure/property analysis for nascent powders having unique morphologies,[25−28] including fibrils,[29] ribbons,[30] whiskers, globules,[31] and so on.

Interest has also been paid to the lamellar thickening process on annealing. Many efforts[32−37] have been devoted to clarification of the lamellar rearrangement. However, there are still two different paradigms; "accelerated chain motion within lamellae causes chain sliding along the lamellar normal", or "recrystallization after partial melting of thinner lamellae causes later creation of thicker lamellae during heating". Both concepts involve their own problems; for example, in the former case, neither a crystallization exotherm nor crystallinity increase during heating has been observed. In the latter case, a sudden increase in lamellar thickness with annealing temperature below the sample melting for solution-grown crystals cannot be interpreted, because this assumed melting/recrystallization system is based on the similarity of gradual lamellar thickness increasing with annealing temperature and melt−crystallization temperature. This discontinuous behavior of lamellar thickening is recently ascribed to a "lamellar doubling" phenomenon during heating.[37]

Such a lamellar rearrangement will be prevented by hindered molecular motion caused by entanglements located in the interfacial region. These entanglements connect the crystalline lamellae through the amorphous phases, which also tie between the crystalline and amorphous phases. Actually, the melt-crystallized sample, having numerous entanglements, seldom shows lamellar thickening below the onset of melting, compared to the significance of the less entangled solution-crystallized samples, as described above. Such an entanglement role in lamellar rearrangement may be visualized by the resultant relationship between relaxation and morphological characteristics for the interfacial region. The same type of assignment for relaxation characteristics will be also extended to a new outlook regarding the usual melt−crystallization with entanglements.

The purpose of this work is to clarify the origin of differences in chain relaxation between various morphologies using a solid-state ^{1}H NMR technique. Such information allows an interpretation of changes in molecular motion for both the crystalline and amorphous phases during heating, combined with the resulting structural changes. The effect of trapped entanglements on such molecular motions inside and outside the lamellae will also be discussed.

Experimental Section

Initial Materials. The material tested was an as-polymerized reactor powder of linear UHMW-PE with a viscosity MW (M_v) of 4×10^6. To examine the MW and MW distribution effects on sample molecular motion, a normal MW PE (Lot 1475a) supplied by the National Institute of Standards and Technology was also used. It has weight- and number-average MW's of 5.2 and 1.8×10^4, respectively, with a narrower MW distribution.

Sample Preparation. Solution-crystallized mats were prepared to have less entanglement in their initial morphology. A 0.05 wt % dilute tetralin solution of these PE powders, with 0.1 wt % (based on the polymer) antioxidant of 2,6-di-*tert*-butyl-*p*-cresol, was prepared at the boiling point under a nitrogen gas flow. This polymer concentration is much lower than the overlapping one for the UHMW of $\sim 4 \times 10^6$. The less entangled crystals were precipitated by quenching this tetralin solution in ice water. The crystals suspension, thus obtained, was filtered into a mat and subsequently dried in vacuo at room temperature (RT).

Fully entangled samples were crystallized from the melt. The initial powder samples were heated to 190 °C and held isothermally for 5 min, followed by quenching in ice water. These treatments were carried out under a nitrogen atmosphere.

Measurements. A Perkin-Elmer Pyris 1 was used to analyze the melting behavior. The DSC heating scan was followed to 180 °C at a heating rate of 5−40 °C/min under a nitrogen gas flow. Calibration of DSC characteristics, including the melting temperature and heat of fusion, was made using indium and tin standards at each heating rate.

For TEM observations, the JEOL 1200EMX electron microscope used was operated at 80 kV. The samples were stained by RuO_4 vapor and embedded in epoxy resin. The assembly was cut into thin sections of 60 nm thick, using a Reichert UltraCut S. microtome.

NMR measurements were carried out using a JEOL MU-25 solid-state pulse NMR spectrometer, equipped with a 25 MHz magnetic field. The FID was recorded by the solid-echo method. Data collection was done every 0.2 μs. The dead time before signal sampling was 2 μs. The observed temperature was raised from RT up to the complete sample melting. Before the signal sampling, the sample temperature was held isothermally for 5 min to determine the homogeneous temperature distribution with a sample probe.

Data Analysis of ^{1}H NMR FID. Generally, to fit the observed FID, a series of exponential (Lorentzian) functions (eq 1) are used because the distribution of dipole interaction is expressed by this function. This is true for the solution, melt, and amorphous phases of the polymers. Actually, a PE melt with low MW exhibits a single-exponential curve.[2−5] The relaxation curve shape of amorphous molecular motion still retains the combined exponential types on cooling. On the other hand, Weibullian functions (eq 2)[9,38] are also applicable for the phase with partially restricted motion such as the interfacial phase.[1] Therefore, it is reasonable to introduce the exponential Weibullian functions as the amorphous relaxation.

$$I_3(t) = A_3 \exp\left\{-\frac{k_3 t}{2}\right\} \tag{1}$$

$$I_2(t) = A_2 \exp\left\{-\frac{(k_2 t)^d}{2}\right\} \tag{2}$$

As crystallinity increased, the curve contains a beat on FID.[6−12,39] Figure 1 shows typical ^{1}H NMR FIDs for UHMW-PE samples. Each FID has a beat (a drop and subsequent recovery) at about 20−30 μs. The beat arises from the fact that the distribution of dipole interaction deviates from the exponential function when the molecular motion is extremely restricted. It has been already recognized that this kind of FID can be characterized by multiplication of Gaussian and sine functions expressed as follows:[13]

$$I_1(t) = A_1 \exp\left\{-\frac{(k_1 t)^2}{2}\right\}\frac{\sin bt}{bt} \tag{3}$$

where t is the decay time and I the normalized magnetization intensity. Analytical Fourier transformation of a Pake doublet produces an extremely complicated FID function;[10−12,14] therefore, eq 3 was assumed for crystalline relaxation in this work.

The actual FID was represented by the sum of these functions ascribed to different relaxation systems. Most of the FIDs were fitted by combination of Gauss/Sine and exponential functions. Some FIDs, especially at elevated temperatures,

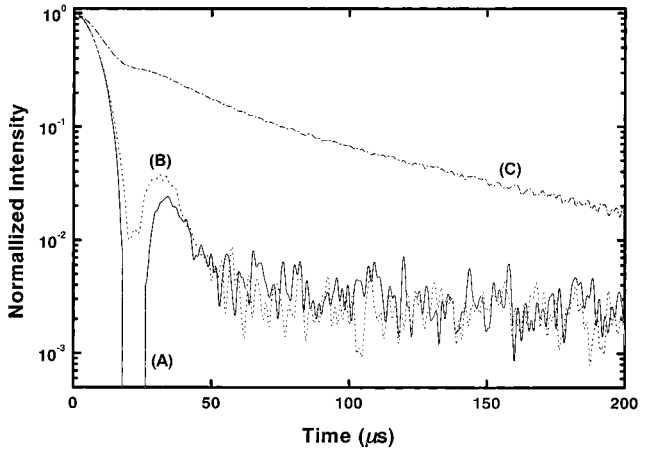

Figure 1. Comparison of FIDs observed at RT for solution-crystallized (A), melt-crystallized (B), and nascent powder (C) samples.

required an addition of another amorphous relaxation for better fitting; thus, three-component resolution (crystalline + two amorphous functions) was attempted. In such a case, the Weibullian function was selected as one of the amorphous decays to reproduce the overall levels of amorphous relaxation. For solution-crystallized and initial powder samples, the Weibullian coefficient d converged into 1, corresponding to the simple exponential decay. However, in the case of a melt-crystallized sample, the intermediate amorphous function was required for desirable profile separation even at RT (see Figure 2), and its Weibullian coefficient gradually deviated from an initial value of 1. A similar three-component detection has been reported for solid-state ^{13}C NMR measurements.[40,41]

Figure 2 illustrates the step-by-step FID resolution procedures into two amorphous and one crystalline relaxation curves for a melt-crystallized sample. First, the longest relaxation was fitted in the time region of 200−400 μs (Figure 2A). After subtraction of the first component from FID, the residual plots were further fitted by another amorphous component (Figure 2B). Resultant crystalline relaxation is well represented by eq 3 (Figure 2C). Because of a negative drop corresponding to this function, the plots in the beat region sometimes did not appear in the log scale in Figure 1 (see the profile of the solution-crystallized sample). The sum of these curves is in good agreement with the observed FID, as shown in Figure 2D.

The obtained crystalline components were Fourier transformed into broad-line spectra for simultaneous evaluation of changes in component ratio and molecular motion. Both Gaussian/Sine (eq 3) and simple exponential decays (eq 1) can be mathematically Fourier transformed on a frequency scale, ν, respectively:

$$F_1(\nu) = \frac{2\pi A_1}{k_1 b}\int_{\nu-b/2\pi}^{\nu+b/2\pi} \exp\left[-\frac{2\pi^2}{k_1^{\,2}}\sigma^2\right] d\sigma \qquad (4)$$

$$F_2(\nu) = \frac{2\sqrt{2}A_2}{\sqrt{\pi}k_2}\frac{1}{\nu^2(4\pi/k_2)^2 + 1} \qquad (5)$$

The integral peak width on a frequency scale was calculated from these broad-line spectra. Each component ratio of crystalline (Gaussian/Sine), intermediate (Weibullian), and relaxed (Lorentzian) amorphous regions was also evaluated as their integral intensities.

Weibullian functions were also Fourier transformed at d = 1 into Lorentzian or 2 into Gaussian peak (in most case, d = 1). When d was between 1 and 2, the approximate transformation into a function combined with these peaks was carried out.

Results

Morphologies. It is well-known that the solid morphologies of semicrystalline polymers are composed of several structural levels of typical modifications: a parallel arrangement of folded molecular chains leading to lamellar crystals, and the actual sample is filled with a sandwiched structure of amorphous layers and such

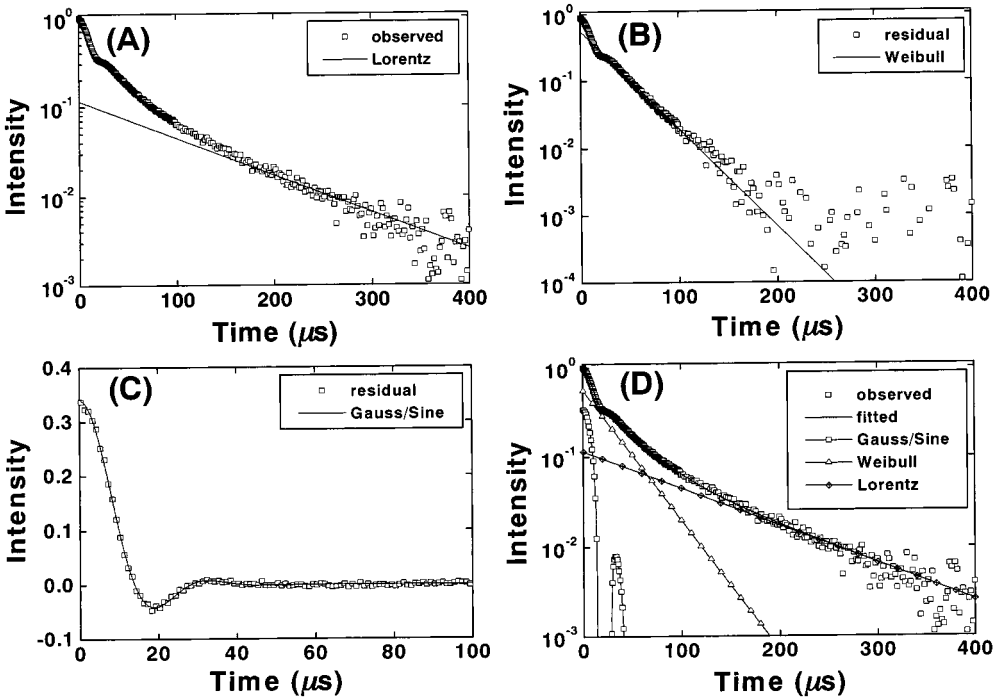

Figure 2. A series of FID resolution procedures into several component decays. The longest relaxation decay, showing a simple exponential function at the longer time scale, was subtracted from the observed FID (A). The other exponential component at the middle time scale was also fitted as amorphous relaxation (B). The final residual curve coincided well with the crystalline Gaussian/Sine function (C). The sum of these resolved profiles was compared with observed plots (D). The data recording was done at RT for melt-crystallized sample.

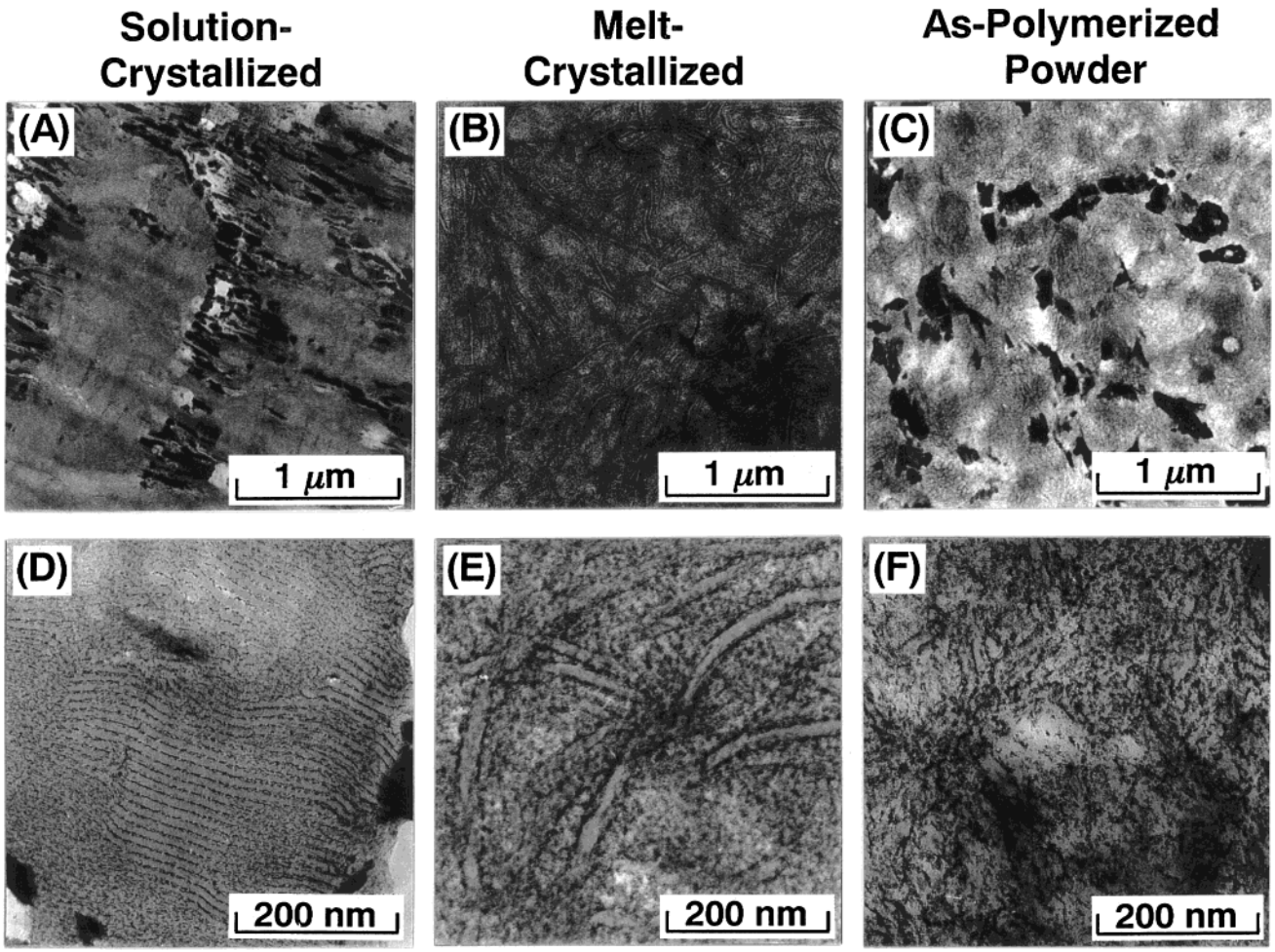

Figure 3. Electron microscopic images of UHMW-PE samples prepared under different conditions: crystallized from solution (A, D), melt (B, E), and as-polymerized (C, F). Top and bottom views correspond to low- and high-magnification images.

lamellae. Melt−crystallization produces a spherulite structure having a distortion of these combined crystal/amorphous phases, but precipitation of separated lamellae is obtained for solution−crystallization. To compare the detailed morphologies of our samples, including the nascent as-polymerized powder structure, direct TEM observations were made. Figure 3 shows the sets of TEM images for solution-crystallized, melt-crystallized, and initial powder samples. Here, the sets of top and bottom views show low- and high-magnification images, respectively. For solution-crystallized samples (see Figure 3D), the regular stacking of lamellar crystals of ∼10 nm thickness is clearly observable. These crystalline lamellae are located between dark layers, indicating the amorphous region and lie laterally within several micrometers length. For the melt-crystallized sample (see Figure 3B), the random arrangement of curved lamellae consists of a spherulite structure. The lamellar thickness of 30 nm for the melt-crystallized sample is much larger than that for the solution-crystallized mats; however, both crystallization conditions produce lamellar units in the solid state.

In contrast, the powder sample has quite a different morphology, compared to the above conventional solution- or melt-crystallized samples. For the powder morphology, the major structure consists of particles having a radius of ∼0.5 μm, and several fibrils are also observed between these particles, as shown in Figure 3C. It has been widely believed that the origin of these "cobweb" structures, composed of particles and fibrils, is ascribed to the internal expansion stress during polymerization.[25,27] Much polymer product synthesized inside the earlier powder globule causes extensive force, which stretches the outer polymer membrane in the polymerization process. Such a cobweb structure has been observed on the powder surface,[15] but it was uncertain whether this cobweb structure fills the interior of the powder. Our result here confirms that the cobweb is a basic structural unit for as-polymerized PE powder. In the high-magnification image (see Figure 3F), it is found that the powder does not have any typical lamellar morphology but has a domain structure where crystalline domains distribute within the whole powder globule. The domain size has a wide range of several tens of nanometers radius.

^{1}H NMR Spin−Spin Relaxation at RT. These sample structures cause the corresponding characteristics in relaxation behavior. To compare the molecular motion of these samples crystallized under different conditions, FID profiles of these samples are compared in Figure 1. These FIDs were observed at RT. The beats, showing a combination of intensity drop and subsequent recovery, are clearly observed in the 20−30 μs region on these FIDs, especially emphasized for higher crystalline solution-crystallized mats and the initial powder. Comparison on a longer time scale also shows that these highly crystalline samples undergo a rapid decay, indicating that the solution-crystallized and initial powder samples seem to be more rigid than the melt-crystallized one over the entire time region.

Table 1. Summarized Spin−Spin Relaxation Characteristics of Components Resolved from FID Observed at Room Temperature for UHMW-PE Samples[a]

morphologies obtained from	crystalline integral width	amorphous integral width
solution	66.2 kHz (91%)	41.2 kHz (9%)
melt	70.4 kHz (61%)	17.4 kHz (28%) + 5.8 kHz (11%)
polymerization	65.8 kHz (85%)	38.3 kHz (15%)

[a] Value in parentheses represents component ratio for corresponding relaxation.

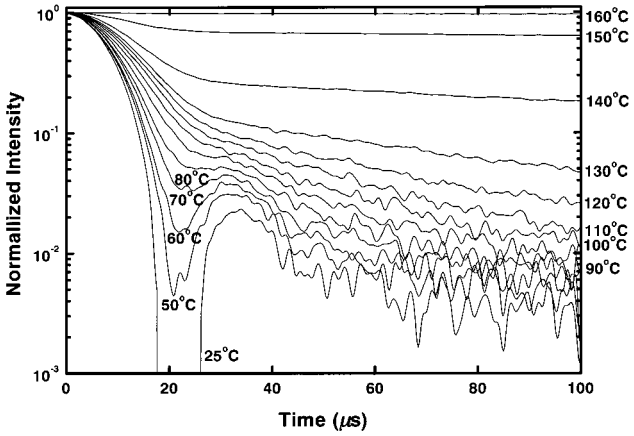

Figure 4. Changes in the FIDs during heating for solution-crystallized UHMW-PE sample.

The relaxation characteristics, obtained by curve fitting and Fourier transformation analysis, are summarized in Table 1. For highly crystalline samples of solution-crystallized mats and the initial powder, the two-component fitting was applicable; however, the melt-crystallized sample required a three-component resolution. The crystalline component ratio, corresponding to the sample crystallinity, was highest for the solution-crystallized sample, followed by the nascent powder sample, and the melt-crystallized sample exhibited the lowest value of ∼50%. The crystalline integral width was slightly smaller for the highly crystalline solution-crystallized and virgin powder samples, suggesting constrained crystalline chain motions for the melt-crystallized sample. Concerning amorphous relaxation, much larger integral widths were obtained for highly crystalline samples, compared to the usual value of 5−10 kHz, which is generally accepted for PE amorphous chain relaxation. This reveals that the amorphous chains in solution-crystallized and initial powder samples were restricted. Such a poor molecular mobility of the amorphous phases for the nascent powder sample has also been observed by ^{13}C NMR measurement.[42] For the amorphous phase of the melt-crystallized sample, the usual relaxation of ∼6 kHz and hindered motion similar to that for the other highly crystalline samples were recognizable. The latter amorphous relaxation could be ascribed to the interfacial molecular motion.

Relaxation Changes during Heating. These relaxation characteristics change with temperature. Morphological differences could be considered distinctive by such a temperature dependence of FID. Figure 4 compares the FIDs obtained during heating from RT to the complete melting for the solution-crystallized sample. The measurement temperature increases from a downward profile to an upward one. As revealed in Figure 4, sample heating gradually suppresses the crystalline beat on the FIDs, and it almost disappears around 110 °C. The decay in the longer time region also becomes gentler with increasing temperature, which indicates the acceleration of molecular motion in the amorphous phase during heating. Other heating scans were also done for other melt-crystallized and initial powder samples.

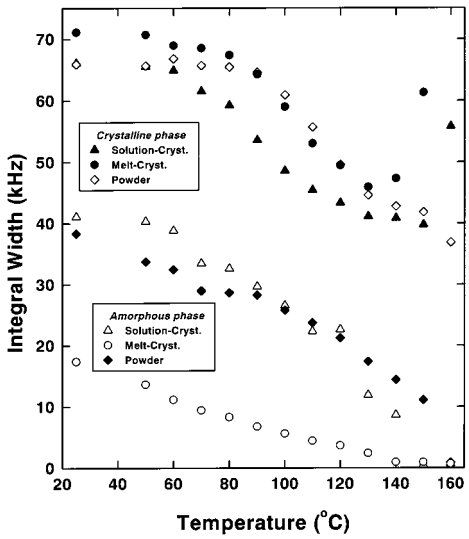

Figure 5. Temperature dependencies of integral widths during heating for solution-crystallized, melt-crystallized, and nascent powder samples of UHMW-PE. Changes in both values for crystalline and amorphous relaxations were plotted for each sample.

The obtained integral width is plotted in Figure 5 for the solution-crystallized, melt-crystallized, and nascent powder samples. Here, the longest relaxation of the melt-crystallized sample was not included because of its smaller amount, compared to another amorphous relaxation. In Figure 5, the higher integral width corresponds to the slower chain motion, such as in crystalline relaxation. If attention is paid to the changes in crystalline relaxation, the characteristics in these different morphologies are attractive. For the solution-crystallized sample, the crystalline integral width is held at the same level below 60 °C, followed by exhibiting a gradual decrease with increasing temperature. This shows that crystalline chain motion starts at a low temperature, reflecting its less entangled lamellar morphology. In contrast, the crystalline chain mobility is accelerated above a higher temperature of 90 °C for the nascent powder sample, leading to a sudden release of chain motion restricted below this critical temperature. This higher releasing temperature may be related to the crystalline domain network structure in its initial morphology (see Figure 3F). For poorly crystalline melt-crystallized sample, relatively larger integral widths are obtained below 90 °C, compared to the other morphologies. This origin will be discussed later.

Concerning the amorphous relaxation, every sample exhibits a successive reduction of integral width, and amorphous molecular motion was gradually accelerated during heating from RT up to the sample melting, independent of the sample morphology. When the amorphous integral width values are compared among these samples, it is found that highly crystalline solution-crystallized and nascent powder samples have values twice that of the melt-crystallized sample over the entire temperature region tested in Figure 5. These comparisons show that the amorphous chain motion is

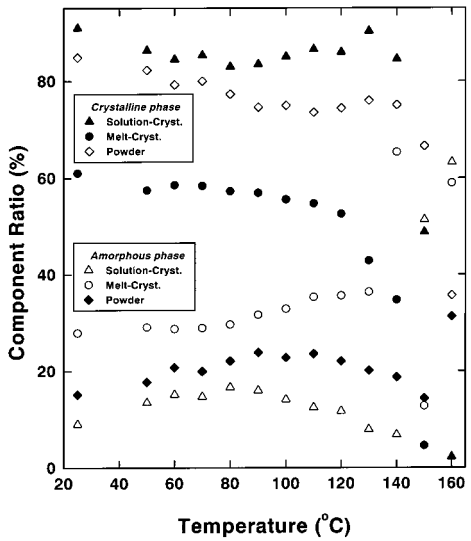

Figure 6. Temperature dependencies of component ratios during heating for solution-crystallized, melt-crystallized, and nascent powder samples for UHMW-PE.

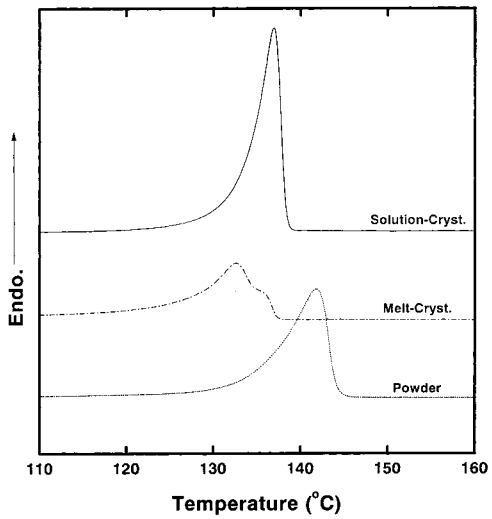

Figure 7. Comparison of DSC melting behavior scanned for solution-crystallized, melt-crystallized, and nascent powder samples of UHMW-PE. The observed heating rate was 10 °C/min.

restricted for the former samples. As these results were summarized, the common characteristics for nascent powder morphology could be recognized as restricted chain motions in both crystalline and amorphous phases.

The above FID resolutions also give component ratios of both crystalline and amorphous phases, as plotted in Figure 6. DSC profiles recorded at 20 °C/min for these samples are also shown in Figure 7, compared with such crystallinity changes during heating as evaluated by ^{1}H NMR. For the melt-crystallized sample, the crystallinity slightly decreases at the level of ~60% but abruptly drops around 120 °C, followed by reaching around 0% crystallinity at 150 °C, due to the complete sample melting. This simple crystallinity decreasing of melt-crystallized PE has been detected by Kristiansen et al.,[12] based on their theoretical ^{1}H NMR profile analysis. These crystallinity changes coincide well with DSC melting behavior for the melt-crystallized sample, having a low-temperature tail with a relatively lower onset and peak melting temperatures (see Figure 7). Similar slight crystallinity decreasing at the early stage of

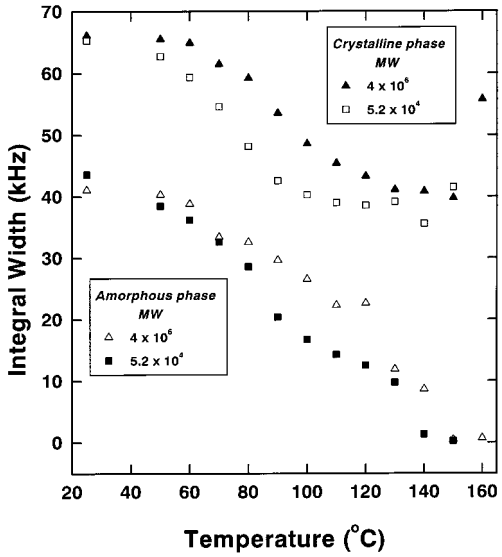

Figure 8. Temperature dependencies of integral width during heating for solution-crystallized normal MW-PE sample. For comparison, data for solution-crystallized UHMW-PE were also included.

heating was also detectable for solution-crystallized and nascent powder samples. However, the difference between these highly crystalline samples lies in each critical temperature, where the crystallinity decrease was limited: 60 °C for the solution-crystallized sample and 90 °C for the initial powder. These critical temperatures corresponded to those observed in the integral width changes in Figure 5 for both samples. It should be noted that the following crystallinity recovery is recognized beyond such a critical temperature for the solution-crystallized sample. This crystallinity reversing can be attributed to the lamellar rearrangement during the heating process. In DSC measurements, any exotherm caused by lamellar rearrangement has never been observed, which was a long-standing question on interpretation of the annealing process for semicrystalline polymers. Combination of synchronized evaluations of both chain mobility and component ratio on the same molecular scale, characterized by ^{1}H NMR relaxation, shows a clear evidence of lamellar rearrangement.

MW Effects on Relaxation Changes. These relaxation changes during heating are also influenced by the sample MW even if the corresponding morphologies crystallized under the same conditions are compared. Here, the FID changes during heating were compared between solution-crystallized normal MW-PE, having a weight-average MW around 5.2×10^4, and UHMW-PE. It was confirmed that the solution-crystallized sample of this normal MW-PE has a lamellar stacked morphology with a periodicity of ~10 nm thickness, which is quite similar to that of UHMW-PE. Compared with the profile changes during heating for solution-crystallized UHMW-PE, the beat disappears at a lower temperature around 70 °C for normal MW-PE (profiles are not shown). Raising the temperature seems to be more effective for the progress of crystalline chain relaxation for a normal MW-PE sample.

Figures 8 and 9 respectively show the MW dependence of the changes in resolved integral width and component ratio during heating. Data collected for solution-crystallized UHMW-PE, which are the same as those shown in Figures 5 and 6, are also included. Decreasing of the crystalline integral width for a normal

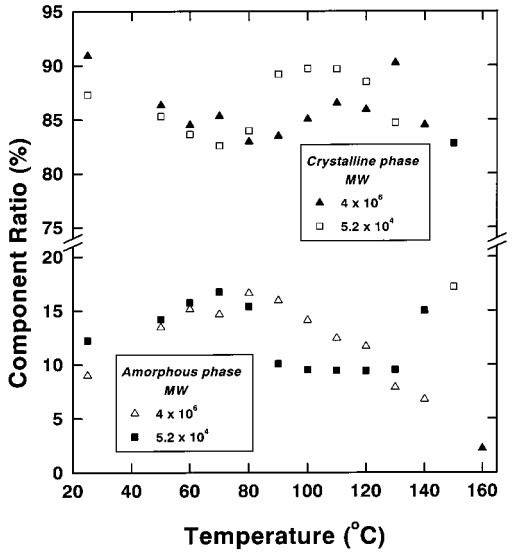

Figure 9. Temperature dependencies of component ratio during heating for solution-crystallized normal MW- and UHMW-PE samples.

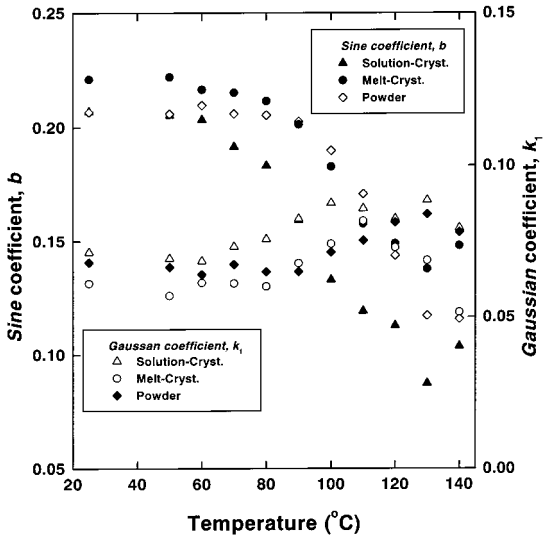

Figure 10. Changes in Gaussian (k_1) and sine coefficients (b) as a function of temperature during heating for solution-crystallized, melt-crystallized, and nascent powder samples for UHMW-PE.

MW-PE sample starts just above RT. At a higher temperature around 110 °C, a saturation of the crystalline width value is recognized for a normal MW-PE sample, but it is not apparently detectable until the sample melting for the UHMW-PE sample. Both MW samples exhibit similar trends of decreasing crystalline width with increasing temperature; however, the above features indicate a low-temperature side shift in the profile change for a normal MW sample. This difference is ascribed to the MW effect on relaxation behavior. Shorter chains allow the ease of molecular relaxation even in the solid-state lamellar morphology, compared to the case of longer chains. As for the amorphous relaxation, increased temperature causes reduction of the integral width for both MW samples. Plots are duplicated, except in the temperature range from 80 to 120 °C, where the lower values are obtained for a normal MW-PE sample. Such a difference is similar to that of the crystalline integral width in this temperature range.

The temperature dependence of the component ratio was also influenced by the sample MW difference. As shown in Figure 9, crystallinity trends reveal a low-temperature side shift for a normal MW sample, compared to a UHMW sample. This is quite similar to that of the integral width change in Figure 8. Also, these characteristics agreed with the endotherm shift in the observed DSC profiles. Both the temperatures of starting crystallinity development and reaching a maximum value for a normal MW sample are lower than those for a UHMW sample, which suggests that the lamellar rearrangement is accelerated at a lower temperature for low MW lamellar crystals, compared to high MW samples. However, it should be noted that the crystallinity recovery is still clearly observable for solution-crystallized normal MW sample.

Discussion

Changes in amorphous relaxation behavior with rising temperature exhibited a monotonic reduction of the integral width, independent of sample morphology and MW, while a crystalline relaxation change revealed unique and individual characteristics for each sample going through different processes during heating. Thus, our interests was concentrated on crystalline relaxation behavior to clarify the origin of the relationship between chain relaxation and sample morphologies.

Factor Predominant for Crystalline Relaxation. To characterize such distinctions of crystalline relaxation systems for the samples having different morphologies, which factor dominates the crystalline relaxation was examined. The crystalline decay function composed of the Gaussian/Sine function, assumed in this work, has two individual coefficients: k_1 and b. Changes in these factors during heating are plotted in Figure 10 for solution-crystallized, melt-crystallized, and powder samples of UHMW-PE. Here, the k_1 coefficients gradually increase with temperature, independent of sample morphology, which should cause an increase in the integral width. In fact, this trend is opposite to that in Figure 5; thus, the effects of k_1 coefficients on crystalline integral width changes are negligible. Instead, it is clearly found that the inclination of the b factor is quite similar to that of the crystalline integral width changes in Figure 5. Namely, the complicated behavior in crystalline relaxation is predominantly defined by the b factor. As shown in eq 4, the decrease in the b coefficient leads to a parallel reduction of the integral width. Especially the fact that their slow decreases start from RT for the melt-crystallized sample agree well with each other (compare Figure 5 with Figure 10). Also for the other morphologies, the critical temperatures where the b coefficient and the integral width exhibit reductions are mutually coincident. Finally at elevated temperatures, the b coefficient asymptotically approaches 0. In eq 3, the term $\sin bt/bt$ equals 1 when the b factor is close to 0. This is the case that the beat is not recognizable on observed FIDs in the higher temperature region, as shown in Figure 4. The Gaussian/Sine function well represents crystalline decay whether or not the observed FID includes beats. Therefore, introduction of the Gaussian/Sine function was effective for evaluation of crystalline relaxation characteristics, such as the existence of a beat and its gradual disappearance with increasing temperature.

As described above, a different relaxation process is recognizable in the b coefficient change shown in Figure

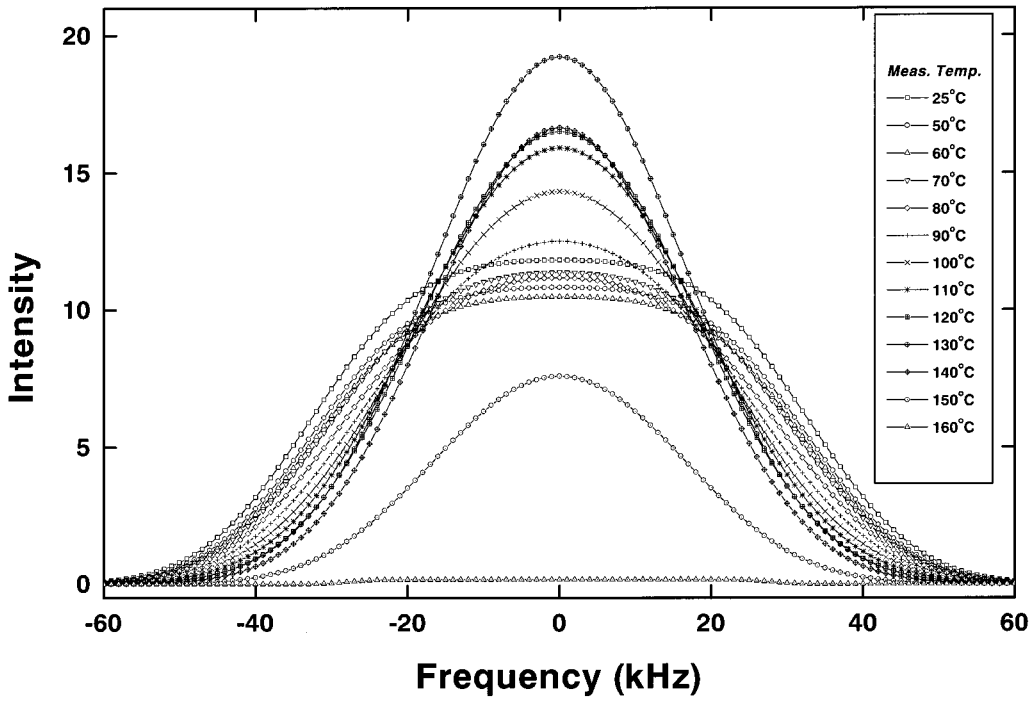

Figure 11. Broad-line spectra Fourier transformed from resolved crystalline decays observed at various temperatures for solution-crystallized sample of UHMW-PE.

10. Particularly, those of the solution-crystallized sample can be clearly divided into three regimes in terms of the effect of temperature on crystalline relaxation. From RT to 60 °C, the constant *b* values were observed (process 1), while a gradual decrease occurred above 60 °C. This trend was accelerated with increasing temperature (process 2), followed by a lower limitation, while the rapid decrease in crystallinity leads to ineffectiveness of the *b* coefficient on the actual FID profile shape (process 3).

Schematic Models for Broad Line Spectra. Considering that integral widths were mainly reflected by the *b* coefficient on the original FID, we thought that these relaxation processes could also be visualized as the changes in the broad-line spectrum shape. Fourier transformation of the crystalline Gaussian/Sine component into the frequency scale gives a trapezoid shape, including not only the integral width but also the crystalline composition indicated by the spectrum integral intensity. These simultaneous evaluations of both molecular motion and crystallinity allow us to summarize the interpretation for crystalline relaxation change during annealing. Figure 11 shows the broad-line spectra converted from the crystalline decays of solution-crystallized UHMW-PE, which exhibits the most typical characteristics of each annealing process among the samples prepared in this work. The crystalline spectrum change during heating for this sample corresponds well to that of the *b* coefficient shown in Figure 10. At the early stage of heating below 60 °C (process 1), the spectrum integral intensity decreases, but the width exhibits no change. From 60 to 130 °C, the spectrum is pushed up as its width decreases (process 2). The final step is that the integral intensity dramatically decreases with almost constant width up to complete sample melting (process 3). These broad-line spectrum changes during heating are schematically shown in Figure 12.

Here, the origins of these relaxation processes can be predicted on the basis of a comparison of the spectrum and sample morphology. The regular stacking of lamellae for solution-crystallized samples likely accompanies folding chains on the lamellar surfaces. These chains are trapped by solid crystals; thus, their molecular motion should be restricted. This indicates that the relaxation of these chains on crystal/amorphous boundaries is considered that of the rigid component, resulting in joining the crystalline relaxation. The origin of the lower integral width values for highly crystalline samples is attributed to this participation of trapped surface amorphous chains in the crystalline relaxation for these samples. The characteristics of spectrum changes during heating could be interpreted for solution-crystallized sample, as follows.

Process 1. The early stage of gradual heating causes the relaxation shift of these interfacial chains into amorphous categories, which leads to the integral intensity (crystallinity) decreasing. However, the residual crystalline molecules inside the lamellae still maintain their hindered molecular motion; thus, the integral width of the spectrum exhibits a constant level.

Process 2. Beyond a critical temperature around 60 °C, a remarkable crystallinity development is observable, which has not been detected by any other crystallinity determination methods. Lamellar growth, causing taking-in of the surrounding amorphous chains, is required for the observed crystallinity increase. Considering the regular stacking of single lamellae of several micrometers wide, this erosion into sandwiched amorphous layer chains progresses parallel to the lamellar normal. The remarkable drop in integral width in this process implies dynamic molecular motion inside the lamellar crystals. If this lamellar development was accomplished only by molecular motion near the surfaces, spectrum narrowing would be less detectable. Therefore, cooperative molecular motion within the entire crystalline lamella from the surface to the interior can be predicted. These violated molecular motions will lead to remarkable lamellar thickening in this temperature range. Through this relaxation process, neither

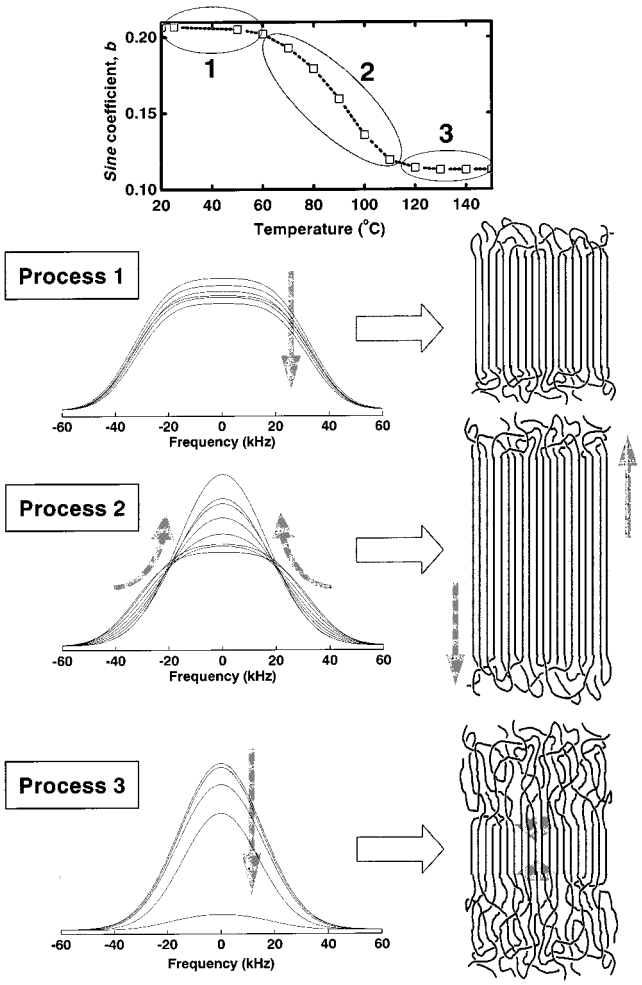

Figure 12. Schematic broad-line spectrum changes through three relaxation processes, divided into different temperature regions.

any partial nor any local melting of lamellae was recognizable even using pulse NMR evaluation at the molecular level.

Process 3. Over 130 °C, rapid progress of partial melting causes a decreasing of the crystalline component. Here, melting does not cause spectrum narrowing. Melting usually starts from the surface due to the higher free energy of the chain folds; thus, the residual crystalline region still retains its saturated molecular motion until the complete melting.

The deviations from the above typical broad-line features for other melt-crystallized and powder samples of UHMW-PE are discussed here. The melt-crystallized sample skipped process 1, due to the limited relaxation of its entangled molecules on the lamellar surfaces, rather than the adjacent reentry folding for the solution-crystallized sample. Thus, even from RT, its structural change during annealing starts as process 2. However, such an entangled surface structure prevents the dynamic molecular motion, which is the major reason that narrowing of the spectrum width is less sensitive to the temperature increasing for the melt-crystallized sample, compared to that for the solution-crystallized sample. Also, process 3 corresponding to the sample melting started at the lower temperature of 120 °C for the melt-crystallized sample, as estimated from relaxation component ratio data (see Figure 6), reflecting its lowest melting temperature confirmed by DSC measurements (see Figure 7).

Annealing of the nascent powder sample passed through process 1. Beyond the critical temperature of 90 °C, dynamic molecular motion starts, as defined by process 2. When such critical temperatures between processes 1 and 2 were compared for solution-crystallized and nascent powder samples, that of the latter was slightly higher than that of the former. These critical temperatures can be regarded as the well-known "crystalline dispersion temperature". This difference indicates the restricted crystalline chain motion for the domain-network structure crystallized during polymerization (see Figure 1F). With increasing temperature in process 2, a narrowing spectrum was detected, but the crystallinity lay at a constant level for the nascent powder sample. This shows that the lamellar thickening is limited for nascent powder morphology. Acceleration of molecular motion within one crystalline domain requires simultaneous dynamic motions with the surrounding domains. This necessity of cooperative relaxation is applicable to the melting process; thus, similar superiority in thermal resistance was recorded as the highest melting peak temperature for this initial powder.

Conclusions

The UHMW-PE crystallized from the solution and the melt or during polymerization had lamellar stacking and spherulites or nascent crystalline domain structures, respectively, as revealed by direct TEM observation. Reflecting each morphology, characteristic FIDs were observed. These contained three components, corresponding to relaxation of crystalline, intermediate, and amorphous chains. Each FID was reasonably analyzed by combination of two types of decay functions: Gauss/Sine and exponential functions. The Gauss/Sine function proposed was successfully applicable to the FID of a crystalline component showing beats. The other two components were reproduced well by Lorentzian and Weibullian decays.

The cystallinity, evaluated as the component ratio of crystalline relaxation at RT, was higher for as-polymerized and solution-crystallized samples than for a melt-crystallized sample. MW effects were recognized for the temperature dependence of relaxation behavior. The integral widths of both amorphous and crystalline chains start to decrease at lower temperature for a normal MW sample, compared to a UHMW sample.

Through these different morphologies or MW, a typical relaxation change during heating could be extracted. Even on heating to the sample melting, the intermediate and amorphous relaxations progressed monotonically. However, the temperature dependence of relaxation behavior for a crystalline chain could be divided into three regimes. Factor *b* of the sine function was most sensitive to such regime transitions. In the temperature region between RT and 60−90 °C, the *b* factor lies at a constant level (process 1). However, its significant reduction was accelerated over the above critical temperature (process 2). On starting the sample melting, the *b* factor became ineffective for evaluating crystalline relaxation, due to rapid decreasing of the crystallinity in this temperature range (process 3).

The crystalline broad-line spectrum, Fourier transformed from resolved Gauss/Sine profiles, emphasized the difference in such crystalline relaxation behavior between sample morphologies examined in this work. This analytical technique visualized the actual crystal-

linity increment on lamellar thickening, which has still not been observed by other methods for crystallinity determination. The advantage of the ^{1}H NMR technique is ascribed to its relaxation analysis on the chain segment scale, which could evaluate both crystalline and amorphous components separately.

For solution-grown crystals and nascent powder samples, the crystalline relaxation had all of these three processes; however, the critical temperature between processes 1 and 2 was higher for the latter morphology. In contrast, melt-grown crystals did not show process 1 and directly led to process 2 upon heating. These revealed that relaxation of the chains around the lamellar surface initiates the chain sliding inside the lamellae without any partial melting, causing the well-known lamellar thickening, for higher crystalline samples. For melt-crystallized samples, the higher density of entanglements trapped on the lamellar surface intercept such a boundary relaxation; thus, lamellar thickening may not be induced. These results imply that the trapped entanglements also play an important role in lamellar rearrangement during annealing.

Acknowledgment. The authors express their thanks to Mr. T. Ikeda in JEOL for kind measurements of NMR and valuable suggestions on profile analysis.

References and Notes

(1) Kenwright, A. M.; Say, B. J. In *NMR Spectroscopy of Polymers*; Ibbett, R. N., Ed.; Chapman and Hall: London, 1993.
(2) Folland, R.; Charlesby, A. *J. Polym. Sci., Polym. Lett. Ed.* **1978**, *16*, 339.
(3) Folland, R.; Charlesby, A. *Eur. Polym. J.* **1979**, *15*, 953.
(4) Koch, H.; Bachus, R.; Kimmich, R. *Polymer* **1980**, *21*, 1009.
(5) Brereton, M. G.; Ward, I. M.; Boden, N.; Wright, P. *Macromolecules* **1991**, *24*, 2068.
(6) Klüver, W.; Ruland, W. *Prog. Colloid Polym. Sci.* **1978**, *64*, 255.
(7) Bergmann, K. *Polym. Bull.* **1981**, *5*, 355.
(8) Bergmann, K.; Schmiedberger, H.; Unterforsthuber, K. *Colloid Polym. Sci.* **1984**, *262*, 283.
(9) Dadayli, D.; Harris, R. K.; Kenwright, A. M.; Say, B. J.; Sunnetcioglu, M. M. *Polymer* **1994**, *35*, 4083.
(10) Hansen, E. W.; Kristiansen, P. E.; Pedersen, B. *J. Phys. Chem. B* **1998**, *102*, 5444.
(11) Kristiansen, P. E.; Hansen, E. W.; Pedersen, B. *J. Phys. Chem. B* **1999**, *103*, 3552.
(12) Kristiansen, P. E.; Hansen, E. W.; Perdersen, B. *Polymer* **2000**, *41*, 311.
(13) Abragam, A. *Principles of Nuclear Magnetism*; Clarendon: Oxford, 1961.
(14) Look, D. C.; Lowe, I. J.; Norhtby, J. A. *J. Chem. Phys.* **1966**, *44*, 3441.
(15) Engelsberg, M.; Lowe, I. J. *Phys. Rev. B* **1974**, *10*, 822.
(16) Pake, G. E. *J. Chem. Phys.* **1948**, *16*, 327.
(17) Gutowsky, H. S.; Kistiakowsky, G. B.; Pake, G. E.; Purcell, E. M. *J. Chem. Phys.* **1948**, *17*, 972.
(18) Gutowsky, H. S.; Pake, G. E. *J. Chem. Phys.* **1950**, *18*, 162.
(19) Loboda-Čačkovič, V. J.; Hosemann, R.; Wilke, W. *Kolloid Z. Z.* **1969**, *235*, 1263.
(20) Phaovibul, O.; Loboda-Čačkovič, J.; Čačkovič, H.; Hosemann, R. *Makromol. Chem.* **1974**, *175*, 2991.
(21) Kitamaru, R.; Horii, F.; Hyon, S.-H. *J. Polym. Sci., Polym. Phys. Ed.* **1977**, *15*, 821.
(22) Bergmann, K. *J. Polym. Sci., Polym. Phys. Ed.* **1978**, *16*, 1611.
(23) Bassett, D. C. *Principles of Polymer Morphology*; Cambridge University Press: London, 1981.
(24) Wunderlich, B. *Macromolecular Physics*; Academic Press: New York, 1973; Vol. 1.
(25) Graff, R. J. L.; Kortleve, G.; Vonk, C. G. *J. Polym. Sci., Polym. Lett.* **1970**, *8*, 735.
(26) Tervoort-Engelen, Y. M. T.; Lemstra, P. J. *Polym. Commun.* **1991**, *32*, 343.
(27) Nooijen, G. A. H. *Eur. Polym. J.* **1994**, *30*, 11.
(28) Uehara, H.; Nakae, M.; Kanamoto, T.; Ohtsu, O.; Sano, A.; Matsuura, K. *Polymer* **1998**, *39*, 6127.
(29) Keller, A.; Willmouth, F. M. *Makromol. Chem.* **1969**, *121*, 42.
(30) Moñoz-Escalona, A.; Parada, A. *J. Cryst. Growth* **1980**, *48*, 250.
(31) Kakugo, M.; Sadatoshi, H.; Sakai, J.; Yokoyama, M. *Macromolecules* **1989**, *22*, 3127.
(32) Grubb, D. T.; Liu, J. J.-H.; Caffrey, M.; Bilderback, D. H. *J. Polym. Sci., Polym. Phys. Ed.* **1984**, *22*, 367.
(33) Kawaguchi, A.; Ichida, T.; Murakami, S.; Katayama, K. *Colloid Polym. Sci.* **1984**, *262*, 597.
(34) Sadler, D. M.; Spells, S. J. *Macromolecules* **1989**, *22*, 3941.
(35) Spells, S. J.; Sadler, D. M. *Macromolecules* **1989**, *22*, 3948.
(36) Spells, S. J.; Hill, M. J. *Polymer* **1991**, *32*, 2716.
(37) Rastogi, S.; Spoelstra, A. B.; Goossens, J. G. P.; Lemstra, P. J. *Macromolecules* **1997**, *30*, 7880.
(38) Brereton, M. G. *J. Chem. Phys.* **1991**, *94*, 2136.
(39) Cohen-Addan, J. P.; Feio, G.; Peguy, A. *Polym. Commun.* **1987**, *28*, 252.
(40) Kuwabara, K.; Kaji, H.; Horii, F.; Bassett, D. C.; Olley, R. H. *Macromolecules* **1997**, *30*, 7516.
(41) Chen, W.; Fu, Y.; Wunderlich, B.; Cheng, J. *J. Polym. Sci., Polym. Phys. Ed.* **1994**, *32*, 2661. (b) Cheng, J.; Fone, M.; Reddy, V. N.; Schwartz, K. B.; Fisher, H. P.; Wunderlich, B. *J. Polym. Sci., Polym. Phys. Ed.* **1994**, *32*, 2683. (c) Fu, Y.; Chen, W.; Pyde, M.; Londono, D.; Annis, B.; Boller, A.; Habenschuss, A.; Cheng, J.; Wunderlich, B. *J. Macromol. Sci., Phys.* **1996**, *B35*, 37.
(42) Morin, F. G.; Delmas, G.; Gilson, D. F. R. *Macromolecules* **1995**, *28*, 3248.

MA9918957